

# Crystal Structures and Magnetic and Gas-Occlusion Properties of Microporous Materials Containing Infinite Chains of Mononuclear Metal (Cu(II), Zn(II), and Ni(II)) Dicarboxylates Unit

Tetsushi Ohmura, Wasuke Mori,\* Mari Hasegawa, Tohru Takei, Toshiya Ikeda, and Eiko Hasegawa

Department of Chemistry, Faculty of Science, Kanagawa University, Hiratsuka, Kanagawa 259-1293

(Received December 20, 2002)

A new series of microporous materials containing infinite chains of a mononuclear metal (Cu(II), Zn(II), Ni(II))-pyridine unit bridged by dicarboxylates (copper(II) terephthalate-pyridine **1a**, copper(II) terephthalate-4-phenylpyridine **1b**, zinc(II) fumarate-pyridine **2a**, zinc(II) terephthalate-pyridine **2b**, nickel(II) fumarate-pyridine **3a**, and nickel(II) terephthalate-pyridine **3b**) have been prepared. These complexes, which have a regular one-dimensional structure, occlude large amounts of gases. The maximum amount of N<sub>2</sub> gas is 0.7–10.7 mole per mole of metal(II) salt, indicating the presence of a large number of micropores. A porous structure, which is formed by stacking and self-assembly of the linear metal(II) dicarboxylates, was determined by X-ray crystallography. We have elucidated the paramagnetic properties of **1a**, **1b**, **3a**, and **3b** by magnetic measurement (SQUID), whereas **2a** and **2b** were found to be diamagnetic. The magnetic susceptibilities of **1a** and **1b** obey the Curie-Weiss law over the range of 70–300 K ( $\theta = -1.4$  K and  $\theta = +5.5$  K, respectively); the obtained Weiss constants ( $\theta$ ) indicate the existence of small antiferromagnetic interactions (**1a**) and ferromagnetic interactions (**1b**). The different magnetic behaviors between **1a** and **1b** demonstrate that hydrogen bonding between the carboxylate groups and coordinated water molecules plays an important role in determining the bridge geometries and super-exchange interaction between the Cu(II) ions through the Cu–O–C–O–H–O–Cu pathways. In contrast to those of the copper(II) complexes, the magnetic susceptibilities of **3a** and **3b** obey the Curie law.

The mineral zeolite was reported by Cronstedt in 1756 and Damour in 1840.<sup>1</sup> In the 20th century, numerous porous compounds (either natural or artificial) became recognized. Zeolite, porous silica, clay, activated carbon, carbon fabric, etc., are well-known classical porous materials.<sup>2</sup> They are classified by their components (organic and inorganic), the degree of crystallization, pore size, and function.

In recent years, metal-organic frameworks have received considerable attention as new and attractive materials in gas storage, ion exchange, and as potential catalysts. Previously, we reported that copper(II) dicarboxylates,<sup>3</sup> molybdenum(II) dicarboxylates,<sup>4</sup> and ruthenium(II,III) dicarboxylates<sup>5</sup> reversibly occluded large amounts of gases, such as N<sub>2</sub>, Ar, O<sub>2</sub>, CH<sub>4</sub>, and Xe. The uniform linear micropores of these adsorbents were assumed as having been constructed by the stacking or bonding of two-dimensional lattices of dinuclear transition-metal dicarboxylates. Many excellent studies of adsorbent porous complexes have also been reported by Yaghi,<sup>6</sup> Kitagawa,<sup>7</sup> Williams,<sup>8</sup> and Fujita.<sup>9</sup>

Recently, it was found that a microporous dicarboxylate polymer, a linear-chain complex of mononuclear copper(II) terephthalate-pyridine **1a**, was followed by a similar system, copper(II) terephthalate-4-phenylpyridine **1b**, zinc(II) fumarate-pyridine **2a**, zinc(II) terephthalate-pyridine **2b**, nickel(II) fumarate-pyridine **3a**, and nickel(II) terephthalate-pyridine **3b** (Chart 1). When guest solvents were released, these complexes, except for **3a**, occluded large amounts of gases, such as N<sub>2</sub> and Ar. The complexes described here can be classified

into two types, based on their crystal structures, as represented schematically by A and B. A preliminary report on the microporous structures, gas-occlusion properties, and magnetic properties of **1a** with the type-A structure has appeared.<sup>10</sup> In this paper, we report on the synthesis of novel adsorbent coordination polymers of mononuclear metal(II) dicarboxylates and their magnetic and gas occlusion properties.

## Experimental

**Synthesis of 1a.** Copper(II) terephthalate-pyridine was synthesized by using a carboxylate-exchange procedure, which we reported previously.<sup>10</sup> Deep-blue, plate-like crystals precipitated out of the solution. [Cu(II)( $\mu$ -O<sub>2</sub>CC<sub>6</sub>H<sub>4</sub>CO<sub>2</sub>)(C<sub>5</sub>H<sub>5</sub>N)<sub>2</sub>(H<sub>2</sub>O)]·C<sub>5</sub>H<sub>5</sub>N·H<sub>2</sub>O **1a**. Anal. Found: C, 53.32; H, 3.82; N, 6.54%. Calcd for C<sub>18</sub>H<sub>16</sub>CuN<sub>3</sub>O<sub>6</sub>: C, 55.14; H, 4.63; N, 8.39%. TG: 16.4% initial weight loss between 23 and 64 °C (16.4% Calcd for C<sub>5</sub>H<sub>5</sub>N).

**Synthesis of 1b.** Copper(II) terephthalate-4-phenylpyridine was synthesized by using a carboxylate-exchange procedure. To a methanol solution (153 mL) of 4-phenylpyridine (155 mg, 0.222 mmol) was added an aqueous solution (10.0 mL) of copper(II) formate tetrahydrate (50.0 mg, 0.222 mmol), an aqueous solution (10.0 mL) of terephthalic acid disodium salt (46.6 mg, 0.222 mmol), and formic acid (18.6 mL). Slow evaporation of the pale-blue eluate gave deep blue, plate-like crystals. [Cu(II)( $\mu$ -O<sub>2</sub>CC<sub>6</sub>H<sub>4</sub>CO<sub>2</sub>)(C<sub>11</sub>H<sub>9</sub>N)<sub>2</sub>(H<sub>2</sub>O)]·2MeOH **1b**. Anal. Found: C, 62.43; H, 4.98; N, 4.54%. Calcd for C<sub>32</sub>H<sub>32</sub>CuN<sub>2</sub>O<sub>7</sub>: C, 61.98; H, 5.20; N, 4.52%. TG: 9.2% initial weight loss between

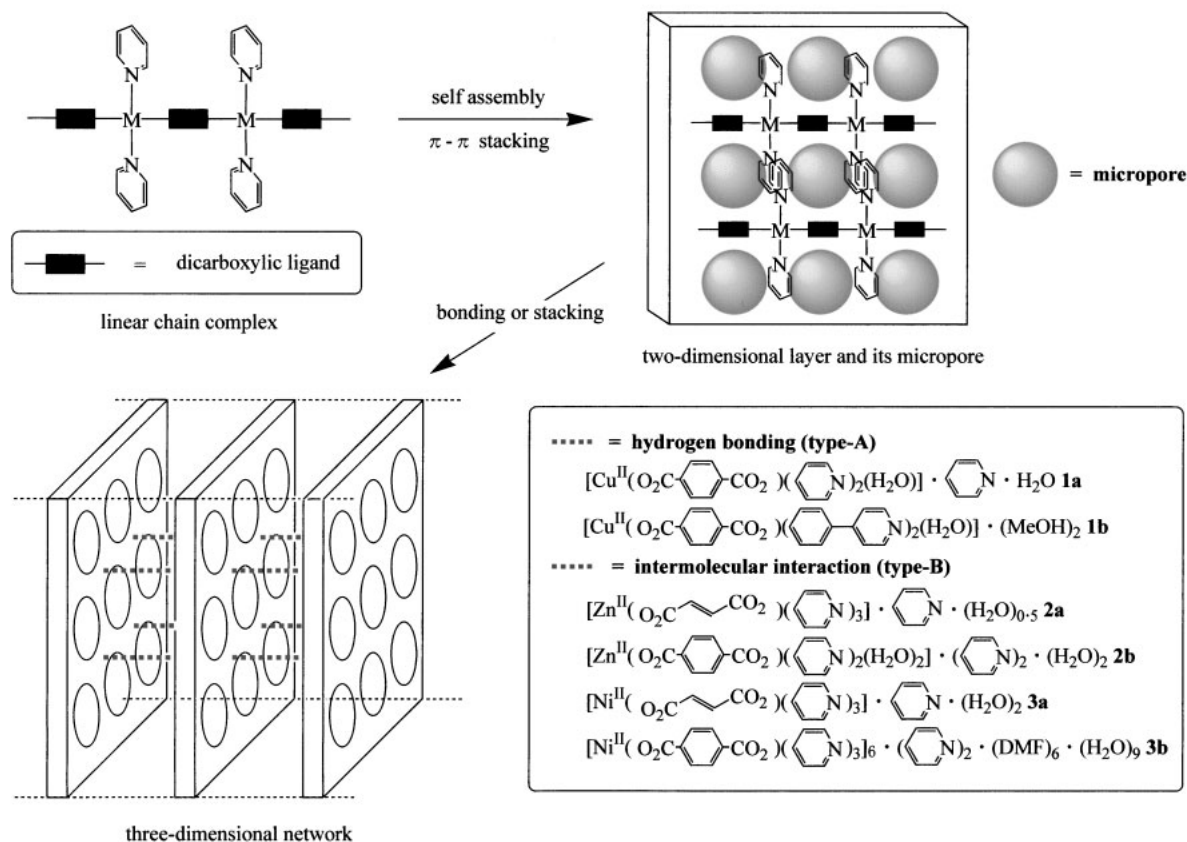


Chart 1.

23 and 116 °C (10.3% Calcd for 2MeOH).

**Synthesis of 2a.** A form of zinc(II) fumarate-pyridine was synthesized as follows. To an aqueous solution (15.0 mL) of zinc(II) nitrate hexahydrate (200 mg, 0.673 mmol) was added a pyridine solution (50.0 mL) of fumaric acid (116 mg, 1.00 mmol). The mixture was then allowed to stand for several days at room temperature, after which colorless, plate-like crystals precipitated out of the solution.  $[\text{Zn}(\text{II})(\mu\text{-O}_2\text{CC}_2\text{H}_2\text{CO}_2)(\text{C}_5\text{H}_5\text{N})_3] \cdot \text{C}_5\text{H}_5\text{N} \cdot 0.5\text{H}_2\text{O}$  **2a**. Anal. Found: C, 57.48; H, 4.62; N, 10.73%. Calcd for  $\text{C}_{24}\text{H}_{23}\text{N}_4\text{O}_{4.5}\text{Zn}$ : C, 57.10; H, 4.59; N, 11.10%. TG: 15.2% initial weight loss between 23 and 116 °C (16.0% Calcd for  $\text{C}_5\text{H}_5\text{N}$ ).

**Synthesis of 2b.** A form of zinc(II) terephthalate-pyridine was synthesized as follows. To an aqueous solution (15.0 mL) of zinc(II) acetate dihydrate (147 mg, 0.673 mmol) was added a pyridine solution (40.0 mL) of terephthalic acid (166 mg, 1.00 mmol). The mixture was then allowed to stand for several days at room temperature, after which colorless plate-like crystals precipitated out of the solution.  $[\text{Zn}(\text{II})(\mu\text{-O}_2\text{CC}_6\text{H}_4\text{CO}_2)(\text{C}_5\text{H}_5\text{N})_2(\text{H}_2\text{O})_2] \cdot (\text{C}_5\text{H}_5\text{N})_2 \cdot 2\text{H}_2\text{O}$  **2b**. Anal. Found: C, 54.40; H, 5.57; N, 8.95%. Calcd for  $\text{C}_{28}\text{H}_{32}\text{N}_4\text{O}_8\text{Zn}$ : C, 54.42; H, 5.22; N, 9.07%. TG: 31.3% initial weight loss between 23 and 83 °C (31.4% Calcd for  $(\text{C}_5\text{H}_5\text{N})_2 \cdot 2\text{H}_2\text{O}$ ).

**Synthesis of 3a.** A form of nickel(II) fumarate-pyridine was synthesized as follows. To a pyridine solution (30.0 mL) of fumaric acid (23.3 mg, 0.201 mmol) was added a DMF solution (20.0 mL) of nickel(II) acetate tetrahydrate (50.0 mg, 0.201 mmol). The mixture was then allowed to stand for several days

at room temperature, after which sky-blue plate-like crystals precipitated out of the solution.  $[\text{Ni}(\text{II})(\mu\text{-O}_2\text{CC}_2\text{H}_2\text{CO}_2)(\text{C}_5\text{H}_5\text{N})_3] \cdot \text{C}_5\text{H}_5\text{N} \cdot 2\text{H}_2\text{O}$  **3a**. Anal. Found: C, 54.53; H, 5.12; N, 10.99%. Calcd for  $\text{C}_{24}\text{H}_{26}\text{N}_4\text{NiO}_6$ : C, 54.89; H, 4.99; N, 10.67%. TG: 22.0% initial weight loss between 23 and 100 °C (21.9% Calcd for  $\text{C}_5\text{H}_5\text{N}$ ).

**Synthesis of 3b.** Another nickel(II) complex **3b** was synthesized in the same manner as **3a**, except that terephthalic acid was used instead of fumaric acid. Sky-blue, plate-like crystals precipitated out of the solution.  $[\text{Ni}(\text{II})(\mu\text{-O}_2\text{CC}_6\text{H}_4\text{CO}_2)(\text{C}_5\text{H}_5\text{N})_3]_6 \cdot (\text{C}_5\text{H}_5\text{N})_2 \cdot 6\text{DMF} \cdot 9\text{H}_2\text{O}$  **3b**. Anal. Found: C, 56.62; H, 5.17; N, 10.58%. Calcd for  $\text{C}_{166}\text{H}_{184}\text{N}_{26}\text{Ni}_6\text{O}_{39}$ : C, 56.65; H, 5.27; N, 10.35%. TG: 22.4% initial weight loss between 23 and 105 °C (21.7% Calcd for  $(\text{C}_5\text{H}_5\text{N})_2 \cdot 6\text{DMF} \cdot 9\text{H}_2\text{O}$ ).

**Physical and Chemical Measurements.** Carbon, hydrogen, and nitrogen analyses were conducted using a Perkin-Elmer PE 2400 seriesII CHNS/O analyzer. Infrared (IR) spectra were measured with a Jasco. Co., FT/IR-300 spectrophotometer in the region of 4000–400  $\text{cm}^{-1}$  using KBr discs. Thermogravimetric/differential thermal analysis was conducted using TG8101D and TAS300 with an aluminum pan in an ordinary atmosphere. Samples were heated between room temperature and 450 °C at 1–4 °C/min. The magnetic susceptibilities at room temperature were measured by the Gouy method (22000 Oe). The temperature dependence of the magnetic susceptibilities was measured by a SQUID magnetometer (Quantum Design, MPMS-5S) in a temperature range of 2–300 K (10000 Oe). The susceptibilities were corrected for the diamagnetism of the constituent atoms by using

Pascal's constants.<sup>11</sup> The effective magnetic moments ( $\mu_{\text{eff}}$ ) were calculated from the equation,  $\mu_{\text{eff}} = 2.83(\chi_{\text{A}}T)^{1/2}$ , where  $\chi_{\text{A}}$  is the atomic magnetic susceptibility.

**X-Ray Crystal Structure Determinations.** The crystal structures of **1a**, **1b**, and **2a** were determined by X-ray diffraction using a Rigaku R-Axis RAPID diffractometer with graphite-monochromated Mo K $\alpha$  radiation. Temperature control was achieved with a temperature control unit. X-ray diffraction data of **2b** were collected on a Rigaku R-Axis RAPID diffractometer by using graphite-monochromated Cu K $\alpha$  radiation. The structures were solved by a direct method using the program SIR-92 and were refined by full-matrix least-squares iterations. Anisotropic thermal parameters were assigned to the Cu, Zn, C, O, and N atoms. The H atoms, except for those of water molecules, were placed at the calculated positions. No disorder was observed in any of the structures.

The crystal structures of **3a** and **3b** were determined by X-ray diffraction using a Bruker APEX diffractometer with graphite-monochromated Mo K $\alpha$  radiation ( $\lambda = 0.7107 \text{ \AA}$ ). The structures were solved by a direct method using the program SHELXS-97, and were refined by full-matrix least-squares iterations. Anisotropic thermal parameters were assigned to the Ni, C, O, and N atoms. The H atoms, except for those of water molecules, were placed at the calculated positions. There is disorder at the C, N, O atoms of the solvent molecules (DMF) in the structure of **3b**, which are divided into two positions with the same weight, respectively.

X-ray powder diffraction data were collected on a Mac Science M18XHF<sup>22</sup>-SRA target Cu diffractometer by using Cu K $\alpha$  radiation. The simulated powder patterns were obtained by using a Cerius2 DIFFRACTION module.

**Gas-Adsorption Measurement.** The temperature dependence of the amounts of occluded N<sub>2</sub> gas for all complexes were determined by a Cahn 1000 electric balance at 20 torr, where 1 torr = (101325/760) Pa, in a temperature range of 77–220 K. After each sample was set in the apparatus, the guest solvents in the pore and on the surface were removed by a treatment in a vacuum. After confirming that a constant weight was reached, nitrogen was dosed into the adsorption chamber. After the equilibrium of adsorption was established, the change in the weight of the sample

was measured. After the buoyancy had been corrected to the obtained amount of the weight change, the absorbed amount of the sample was calculated.

Adsorption isotherms were measured using an ASAP 2010 volumetric adsorption apparatus provided by Micromeritics Co., Ltd. Before adsorption measurements, the samples were degassed under a vacuum at 273 K. Adsorption isotherms were measured in the relative pressure ( $p/p_0$ ,  $p_0$  = saturation pressure) range from  $10^{-6}$  to 0.65.

## Results and Discussion

**Structure Description.** Crystallographic data and other pertinent information are summarized in Table 1. For each structure, we present an ORTEP drawing of the unit containing the copper, zinc, and nickel atoms and all attached atoms, in Figs. 1–6. In each figure, the atomic numbering scheme for the species is defined.

The microporous structures, each of which has a large number of micropores, are shown in Fig. 7. The results suggest that these complexes, except for **3a**, form capillary structures. In all of the complexes, the van der Waals interaction between the pyridine rings of the ligands, the so-called  $\pi$ - $\pi$  stack, may

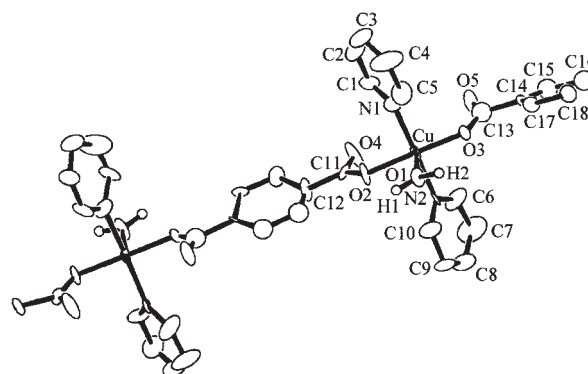


Fig. 1. ORTEP view of **1a** showing the numbering scheme. For clarity, the hydrogen atoms and the solvent molecules (pyridine) have been omitted.

Table 1. Crystallographic Data Collection and Structure Refinement Parameters for **1a**, **1b**, **2a**, **2b**, **3a**, and **3b**

	<b>1a</b>	<b>1b</b>	<b>2a</b>	<b>2b</b>	<b>3a</b>	<b>3b</b>
Chemical formula	CuC <sub>26</sub> H <sub>21</sub> N <sub>4</sub> O <sub>5</sub>	CuC <sub>30</sub> H <sub>24</sub> N <sub>2</sub> O <sub>5</sub>	ZnC <sub>25</sub> H <sub>13</sub> N <sub>3</sub> O <sub>4</sub>	ZnC <sub>28</sub> H <sub>24</sub> N <sub>4</sub> O <sub>4</sub>	Ni <sub>2</sub> C <sub>48</sub> H <sub>44</sub> N <sub>8</sub> O <sub>8</sub>	Ni <sub>6</sub> C <sub>174</sub> H <sub>156</sub> N <sub>24</sub> O <sub>38</sub>
Formula mass/Da	533.02	556.08	484.78	545.9	978.33	3543.49
Space group	<i>Cc</i>	<i>C2/c</i>	<i>P2<sub>1</sub>/n</i>	<i>P2<sub>1</sub>/n</i>	<i>P1</i>	<i>P2<sub>1</sub>2<sub>1</sub>2</i>
<i>a</i> /Å	17.8636(9)	24.908(3)	9.9050(8)	12.368(5)	9.1818(8)	16.1359(11)
<i>b</i> /Å	5.9305(3)	5.8332(5)	17.877(1)	15.382(5)	9.7958(9)	57.178(4)
<i>c</i> /Å	22.001(2)	22.075(2)	13.427(1)	23.340(8)	12.8848(12)	19.4167(13)
$\alpha$ /deg	90.000	90.000	90.000	90.000	90.244(2)	90.000
$\beta$ /deg	114.239(2)	105.628(3)	91.309(2)	91.41(2)	90.017(2)	90.000
$\gamma$ /deg	90.000	90.000	90.000	90.000	90.381(2)	90.000
<i>V</i> /Å <sup>3</sup>	2125.3(2)	3088.8(5)	2376.9(3)	4439.0(2)	1158.86(18)	17914(2)
$\rho_{\text{calcd}}$ /g cm <sup>-3</sup>	1.666	1.196	1.693	1.225	1.402	1.314
<i>T</i> /K	296.0	123.0	203.0	103.0	90.0	90.0
$\lambda$ /Å	0.71069	0.71069	0.71069	1.5419	0.71073	0.71073
<i>R</i> <sup>a</sup>	0.055	0.074	0.049	0.039	0.0336	0.0906
<i>R<sub>w</sub></i> <sup>b</sup>	0.122 <sup>b</sup>	0.124 <sup>b</sup>	0.057 <sup>b</sup>	0.051 <sup>b</sup>	0.0835 <sup>c</sup>	0.2588 <sup>c</sup>
<i>Z</i>	4.0	4.0	4.0	6.0	1.0	4.0
$\mu$ /cm <sup>-1</sup>	10.79	7.44	13.35	14.508	8.75	6.97

a)  $R = \Sigma||F_0| - |F_C||/\Sigma|F_0|$ . b)  $R_w = [\Sigma w(|F_0| - |F_C|)^2/\Sigma w F_0^2]^{1/2}$ . c)  $R_w = [\Sigma(w(F_0^2 - F_C^2)^2)/\Sigma(F_0^2)^2]^{1/2}$ .

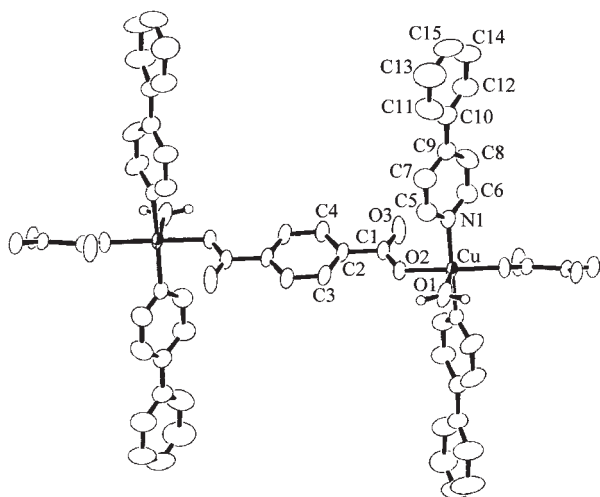


Fig. 2. ORTEP view of **1b** showing the numbering scheme. For clarity, the hydrogen atoms and the solvent molecules (methanol) have been omitted.

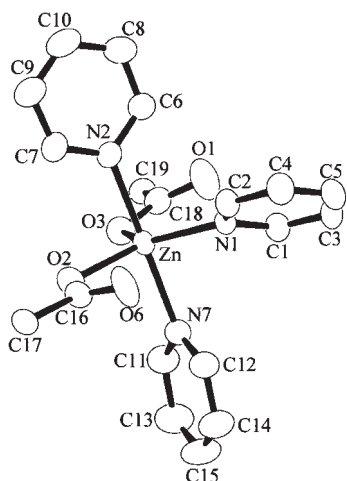


Fig. 3. ORTEP view of **2a** showing the numbering scheme. For clarity, the hydrogen atoms and the solvent molecules (pyridine) have been omitted.

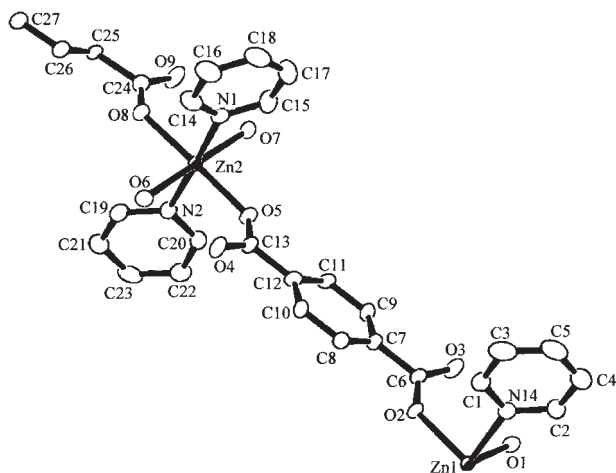


Fig. 4. ORTEP view of **2b** showing the numbering scheme. For clarity, the hydrogen atoms and the solvent molecules (pyridine and water) have been omitted.

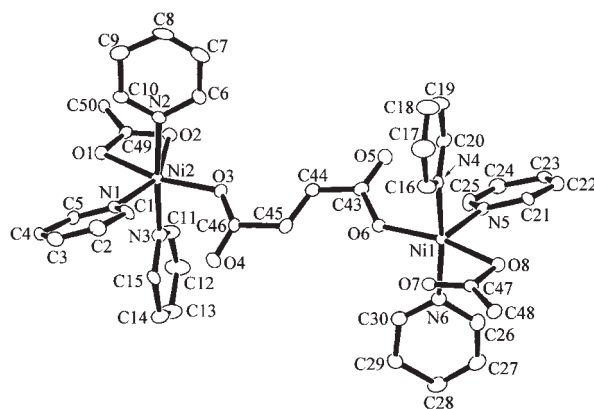


Fig. 5. ORTEP view of **3a** showing the numbering scheme. For clarity, the hydrogen atoms and the solvent molecules (pyridine) have been omitted.

act as a driving force for the self-assembly of the one-dimensional metal(II) dicarboxylates to form two-dimensional lattice structures.

The hydrogen bonding of **1a** and **1b** with the type-A structure are clearly characterized by X-ray crystallography; hydrogen bonding occurs between the two-dimensional layers, through the O atoms of the carboxylate groups and the coordinated water molecules, increasing the structural dimensionality of **1a** and **1b** (Fig. 8).

The crystal structures of **2a**, **2b**, **3a**, and **3b** with the type-B structure contain no coordinated water molecules, and thus no water hydrogen bonding. These structures are constructed by the stacking of two-dimensional lattices (intermolecular interaction), and form very similar capillary structures to that of the type-A (Fig. 9).

In the process of crystallization, the micropores are occupied by molecules of the solvent, as shown in Fig. 10. The guest solvent, such as pyridine and/or water molecules, were removed from the micropores by a treatment in a vacuum. No structural decomposition occurred in the removal of crystal solvents in a vacuum, as illustrated by sharp peaks observed in the X-ray powder diffraction patterns, which is in a good agreement with that of the simulated structures, as shown in Fig. 11. This result suggests no deformation of the crystal frameworks.

**Stability of Complexes.** All of the synthesized complexes were hygroscopic and relatively sensitive to moisture. Analytical data for all of the complexes are in good agreement with a composition having few water molecules.

A TG-DTA analysis showed that the guest solvent was eliminated from the network as the temperature rose (Fig. 12). When the guest solvents were released, the deep-blue **1a** and **1b** changed to the pale-blue **1a'** and **1b'**, capable of occluding gases.<sup>12</sup> These networks with the type-A structure were stable to the initial weight loss of the guest solvent, whereas in the loss of coordinated molecules (water forming hydrogen bonding and pyridine), these complexes exhibited no gas-occlusion properties. On the other hand, when the guest solvents were released, the colorless **2a** and **2b** changed to white **2a'** and **2b'**, capable of occluding gases. Similarly, the sky-blue **3a** and **3b** changed to pale-sky-blue **3a'** and

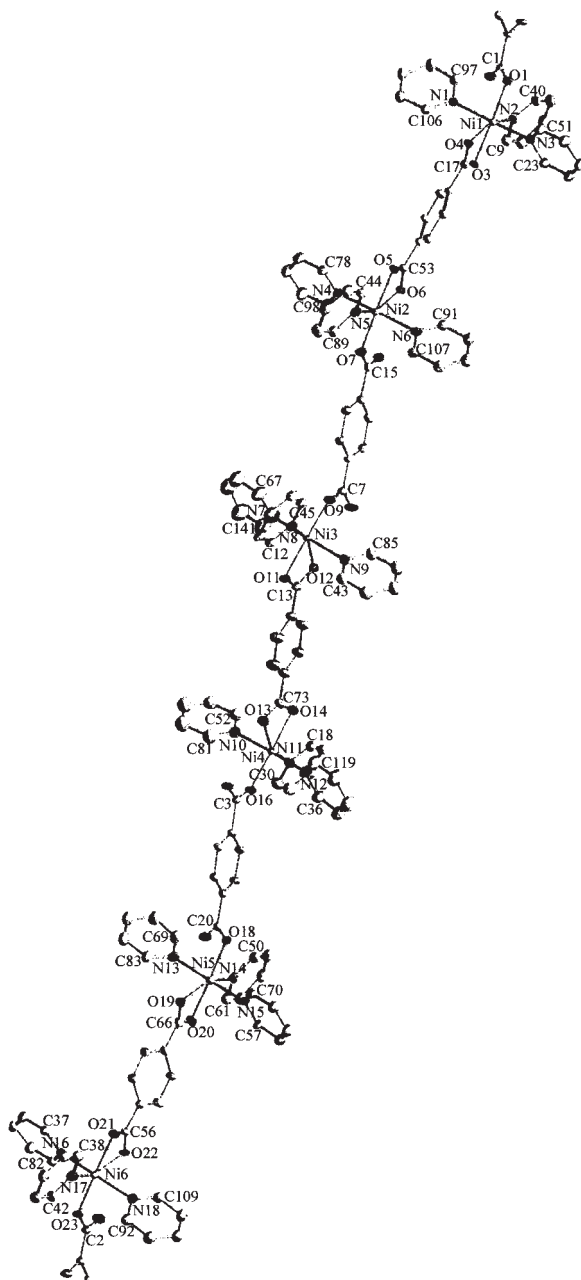


Fig. 6. ORTEP view of **3b** showing the numbering scheme. For clarity, the hydrogen atoms and the solvent molecules (pyridine, DMF, and water) have been omitted.

**3b'**. Complex **3b'** exhibited gas-occlusion properties. These networks with the type-B structure are stable to the initial weight loss of the guest solvent, whereas in the loss of coordinated molecules (pyridine and/or water) these complexes exhibited no gas-occlusion properties.

**IR Spectra.** The IR spectra of all the complexes exhibited very strong-intensity bands in the 1200 and 1700  $\text{cm}^{-1}$  regions. Selected IR spectral data are summarized in Table 2. The bands for **3b** at 1591 and 1381  $\text{cm}^{-1}$  are assigned to the  $\nu_{\text{asym}}(\text{CO}_2)$  and  $\nu_{\text{sym}}(\text{CO}_2)$  stretching modes, respectively, of the bound monodentate end of the terephthalate ligand, as shown in Fig. 6. The 1568  $\text{cm}^{-1}$  band is assigned to the  $\nu_{\text{asym}}(\text{CO}_2)$  stretching mode of the bidentate portion of the

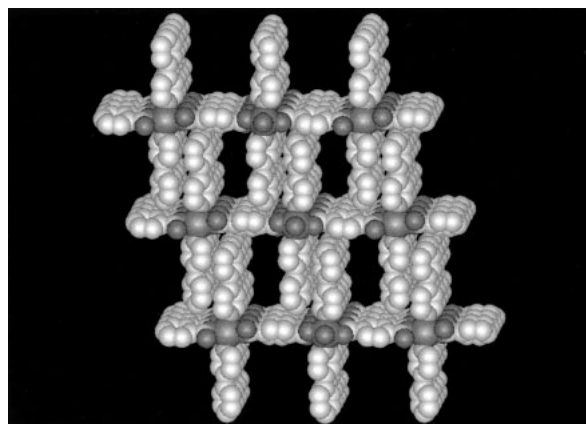


Fig. 7. View of crystal structure of **1b**. For clarity, the hydrogen atoms and the solvent molecules (methanol) have been omitted.

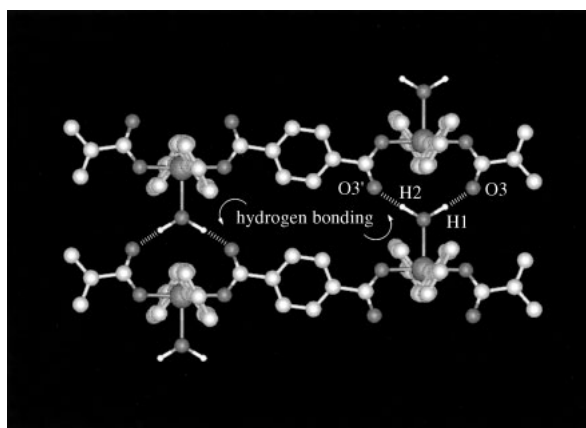


Fig. 8. Hydrogen bonding structure of **1b**. The water hydrogen bonding between the H atoms (H1 and H2) of the coordinated water molecules and the O atoms (O3 and O3') of the carboxylate groups also form a three-dimensional network structure. For clarity, the hydrogen atoms and the solvent molecules (methanol) have been omitted.

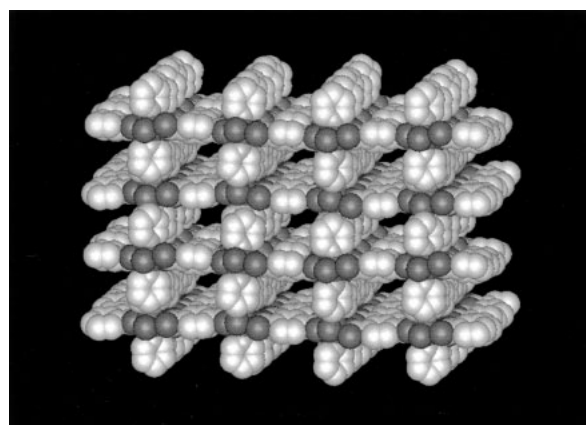


Fig. 9. View of crystal structure of **2b**. For clarity, the hydrogen atoms and the solvent molecules (pyridine and  $\text{H}_2\text{O}$ ) have been omitted.

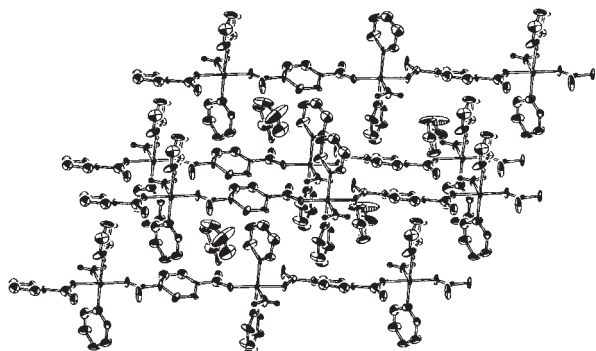


Fig. 10. View of crystal structure of **1a**. The micropores are occupied by molecules of the solvent (pyridine). For clarity, the hydrogen atoms have been omitted.

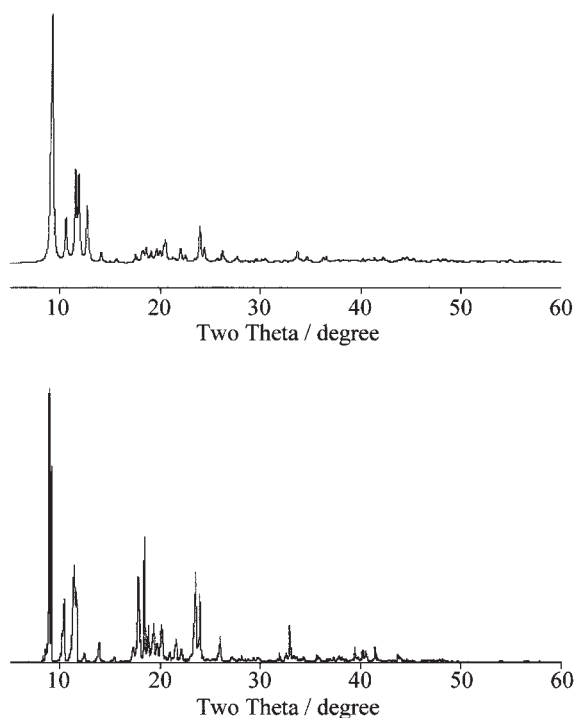


Fig. 11. Simulated (top) and observed (bottom) X-ray powder diffractions patterns of **3b'** at room temperature in a  $N_2$  gas flow.

terephthalate ligand, with the  $\nu_{\text{sym}}(\text{CO}_2)$  mode overlapping that of the monodentate end of the terephthalate ligand. The splitting between the bands of the bound monodentate end is  $\Delta = 210 \text{ cm}^{-1}$ , larger than that for the bidentate end ( $\Delta = 187 \text{ cm}^{-1}$ ). This is consistent with the larger carboxylate O–C–O bond angle of the terephthalate ligand for the monodentate end, as compared to the carboxylate end bidentate to Cu(II), Zn(II), and Ni(II), as shown in Tables 2 and 3. The IR spectrum of **1a** and **1b** with the type-A structure displays  $\Delta = 238$  and  $231 \text{ cm}^{-1}$ , respectively, indicative of a monodentate binding mode where H-bonding occurs with the unbound CO group.<sup>13</sup>

**Gas-Occlusion Properties.** The occlusion of  $N_2$  gas by **1a'** occurs at temperatures below 180 K, with the amount of occluded  $N_2$  gas nearly reaching saturation at 130 K.<sup>10</sup> The maximum amount of occluded  $N_2$  gas for **1a'** was 1.1 mole per

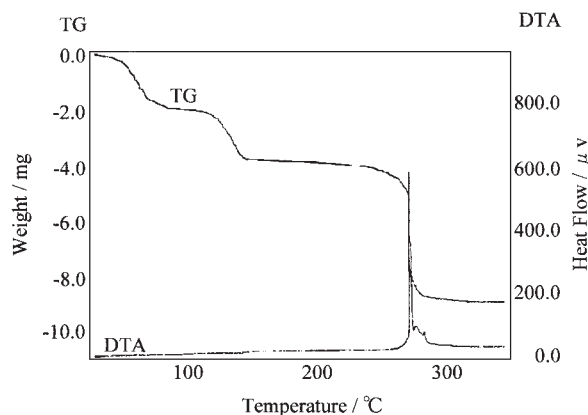


Fig. 12. TG-DTA curves of **1a**. Sample of 11.328 mg, heating in an aluminum pan at  $1.0 \text{ }^\circ\text{C}/\text{min}$ . An initial weight loss of 16.4% at  $64 \text{ }^\circ\text{C}$  for evacuation of the pyridine guests from the micropores, with one pyridine removed per formula unit (16.4% calculated), followed by second weight loss of 4.8% at  $89 \text{ }^\circ\text{C}$ , corresponding to the removal of one coordinated water forming hydrogen bonding per formula unit (3.7% calculated).

Table 2. Selected IR Spectral Data ( $\text{cm}^{-1}$ ) of **1a**, **1b**, **2a**, **2b**, **3a**, and **3b**

Complex	$\nu_{\text{asym}}(\text{CO}_2)$	$\nu_{\text{sym}}(\text{CO}_2)$	$\Delta(\nu_{\text{asym}} - \nu_{\text{sym}})$
<b>1a</b>	1599	1361	238
<b>1b</b>	1593	1362	231
<b>2a</b>	1554	1385	169
<b>2b</b>	1574	1394	180
<b>3a</b>	1551	1389	162
<b>3b</b>	1591, 1568	1381	210, 187

Table 3. Selected Bond Angles (deg) of **1a**, **1b**, **2a**, **2b**, **3a**, and **3b**

<b>1a</b>		<b>3a</b>	
O(2)–C(11)–O(4)H bonds	122(1)	O(1)–C(49)–O(2)*	120.3(8)
O(3)–C(13)–O(5)H bonds	128(1)	O(5)–C(43)–O(6)	122.9(8)
		O(7)–C(47)–O(8)	121.4(8)
<b>1b</b>		<b>3b</b>	
O(2)–C(1)–O(3)H bonds	125.3(7)	O(1)–C(1)–O(2)	128.0(8)
<b>2a</b>		O(3)–C(17)–O(4)*	121.0(7)
O(2)–C(16)–O(6)	124.0(5)	O(5)–C(53)–O(6)*	121.0(8)
O(1)–C(18)–O(3)	124.5(5)	O(7)–C(15)–O(8)	124.7(8)
<b>2b</b>		O(9)–C(7)–O(10)	123.1(8)
O(8)–C(24)–O(9)	126.3(6)	O(11)–C(13)–O(12)*	119.0(8)
O(4)–C(13)–O(5)	126.0(5)	O(13)–C(73)–O(14)*	121.3(9)
O(2)–C(6)–O(3)	126.1(6)	O(15)–C(3)–O(16)	128.7(8)
		O(17)–C(20)–O(18)	129.2(8)
		O(19)–C(66)–O(20)*	122.1(8)
		O(21)–C(56)–O(22)*	120.3(8)
		O(23)–C(2)–O(24)	122.9(8)

\*Bond bidentate end of the terephthalate ligand.

mole of copper(II) salt. Remarkably, **1b'**, **2a'**, **2b'**, and **3b'**, with the exception of **3a'**, displayed the ability to occlude large amounts of gases. X-ray crystallographic analyses revealed that **3a** had “zero-dimensional micropores”, as shown in

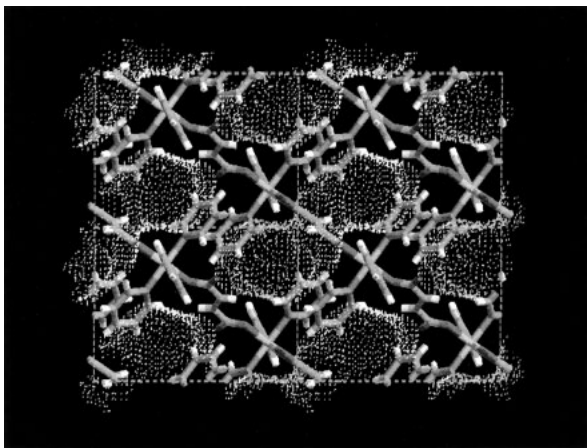


Fig. 13. Crystal structure of **3a**. The probability distribution of loaded gas molecules is pictured as a cloud of dots. For clarity, the hydrogen atoms and the solvent molecules (pyridine) have been omitted.

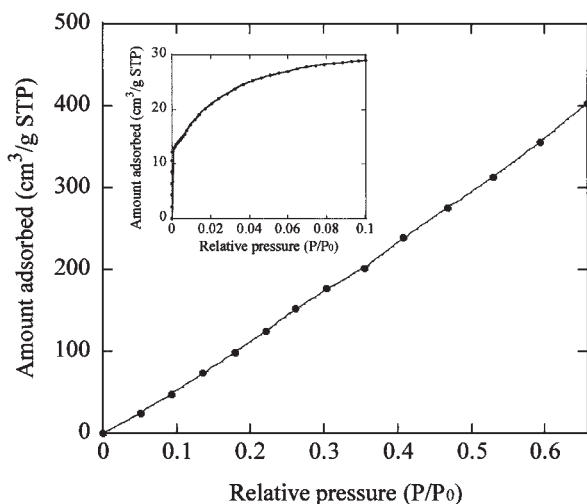


Fig. 14. Adsorption isotherm of **2a'** obtained with an argon gas in the relative pressure range from  $10^{-6}$  to 0.65 at temperature of liquid argon. Adsorption isotherm of **1a'** (type I) is shown in the inset.

Fig. 13, and thus no gas-occlusion properties. Also, the amounts of occluded gas increase with a decrease in the temperature, and finally reached a maximum point at the temperature of liquid nitrogen. The maximum amounts of occluded  $N_2$  gas for **1b'**, **2a'**, **2b'**, and **3b'** were 4.8, 10.6, 2.0, and 0.7 mole per mole of metal(II) atoms, respectively. The crystal structures and gas-occlusion properties suggest that **1b'**, **2b'**, and **3b'** form very similar capillary structures to that of **1a'**.

For **2a'**, an argon adsorption experiment was carried out in the relative pressure range from  $10^{-6}$  to 0.7 (Fig. 14). This complex shows an isotherm of type V according to the BDDT classification.<sup>14</sup> The volume adsorbed increased linearly with an increase in the relative pressure, and exhibited a very high adsorbed volume, thus, indicating a large gas-occlusion capability.

**Magnetic Properties.** To investigate the structure in further detail, the temperature dependences of the magnetic sus-

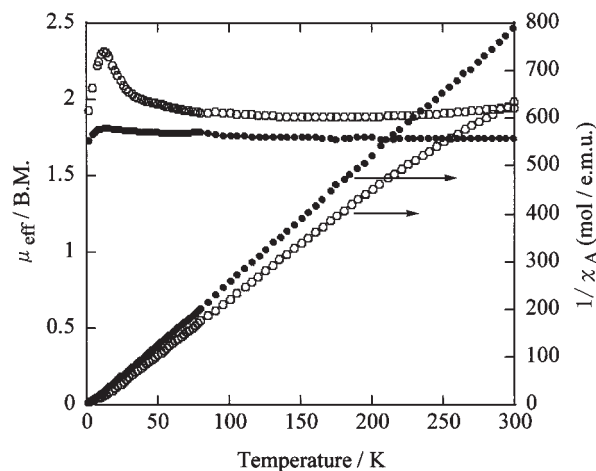


Fig. 15. Temperature dependence of the effective magnetic moments and magnetic susceptibilities for **1a**(●) and **1b**(○).

ceptibilities of **1a**, **1b**, **3a**, and **3b** were measured. In the type-A complexes, in which one copper(II) ion is linked by one dicarboxylate and one coordinated water molecule, two-pathways are provided for a superexchange interaction between copper(II) ions. Fig. 15 shows the temperature dependence of the magnetic susceptibilities and effective magnetic moments. The magnetic susceptibilities of **1a** and **1b** with the type-A structure obey the Curie-Weiss law over the range of 70–300 K ( $\theta = -1.4$  K, and  $\theta = +5.5$  K, respectively); the obtained Weiss constants ( $\theta$ ) indicate the existence of small antiferromagnetic interactions for **1a**, and ferromagnetic interactions for **1b**. The relatively high value of  $\theta$  for **1b** suggests significant ferromagnetic coupling arising from the hydrogen bonding. Also, similar values ( $\theta = +9.0$  K) have been reported for ferromagnetic interactions through the hydrogen bonded pathways in  $[Cu(II)(\mu-O_2CC_6H_5)_2(C_5H_5N)_2(H_2O)]$ .<sup>15</sup> The different magnetic behaviors between **1a** and **1b** demonstrate that the hydrogen bonding between the bridging carboxylate groups and the coordinated water molecules plays an important role in determining the bridge geometries and super-exchange interaction between the Cu(II) ions through the Cu–O–C–O–H–O–Cu pathways. The dihedral angles between the [Cu, O2, O4] and [Cu, O3, O5] planes and between the [Cu, O2, O3] and [Cu, O2', O3'] planes are  $3.4^\circ$  and  $38.4^\circ$  in **1a** and **1b**, respectively. Conversely, it might be suggested that no magnetic interactions exist between the Cu(II) ions through the bridges of terephthalate ligands. The dihedral angles between the [O2(O3), N1, N2] and [C12(C14), C15(C16), C17(C18)] planes and between the [O2, N3, N3'] and [C2(C2'), C3'(C3), C4(C4')] planes are  $69.9$ – $75.5^\circ$  and  $70.6^\circ$  in **1a** and **1b**, respectively. These results suggest that **1a** and **1b** are not affected by magnetic interactions arising from a large distortion of these dihedral angles ( $69.9$ – $75.5^\circ$  and  $70.6^\circ$ ). Consequently, the net ferromagnetic interaction observed for **1b** is due to a weaker antiferromagnetic contribution derived from a large distortion of the Cu–O–C–O–H–O–Cu super-exchange pathway.

Fig. 16 shows the temperature dependence of the magnetic susceptibilities and effective magnetic moments for **3a** and **3b**.

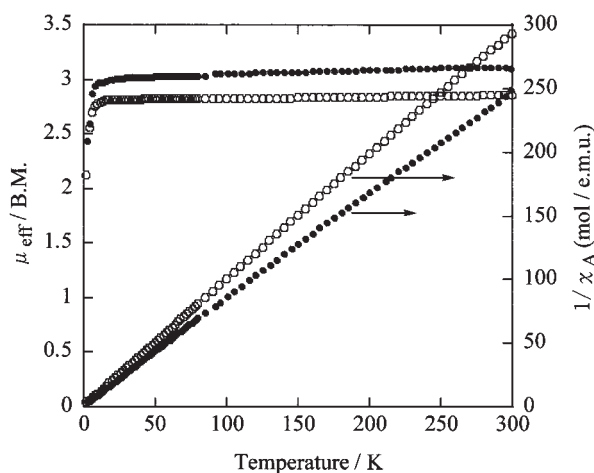


Fig. 16. Temperature dependence of the effective magnetic moments and magnetic susceptibilities for **3a**(●) and **3b**(○).

In contrast to the copper(II) complexes (**1a** and **1b**), the magnetic susceptibilities of **3a** and **3b** with the type-B structure obey the Curie law. Therefore, the magnetic behaviors of **3a** and **3b** with no hydrogen bonding are barely affected by the magnetic interaction between the Ni(II) ions.

### Conclusion

In the present work, we succeeded to synthesize novel adsorbent coordination polymers of mononuclear metal(II) dicarboxylates: copper(II) terephthalate-pyridine **1a**, copper(II) terephthalate-4-phenylpyridine **1b**, zinc(II) fumarate-pyridine **2a**, zinc(II) terephthalate-pyridine **2b**, nickel(II) fumarate-pyridine **3a**, and nickel(II) terephthalate-pyridine **3b**. When guest solvents were released, these complexes (**1a'**, **1b'**, **2a'**, **2b'**, and **3b'**) exhibited a gas-occlusion capability similar to that of copper(II) dicarboxylates, as reported previously.<sup>3</sup> The maximum amounts of occluded N<sub>2</sub> gas for **1a'**, **1b'**, **2a'**, **2b'**, and **3b'** were 1.1, 4.8, 10.6, 2.0, and 0.7 mole per mole of the metal(II) atoms, respectively. Uniform capillaries constructed by the stacking and self-assembly of the linear metal(II) dicarboxylates were determined by X-ray crystallography. Large amounts of gas may be occluded in the capillaries (in the case **2a'** may be also occluded in other site), as shown in Figs. 7, 9–11, 14. In comparison with industrially important adsorbents, such as the well-known zeolite, silica, and activated carbon,<sup>16</sup> the system discovered in the present work is the simplest and most advantageous adsorbent for studying pure and applied chemistry. This statement is true in the following respects: (1) The amounts of occluded gas are very large. (2) No disturbances, such as counterions, are required. (3) The homogeneity of the micropores, which are most probably linear capillaries, and the adsorbed molecules would be distributed as a column. (4) Simplicity to obtain single crystals for microporous polymer of mononuclear metal(II) dicarboxylates. (5) It is possible to synthesize novel adsorbent coordination polymers of mononuclear Ni(II) dicarboxylates, but not dinuclear Ni(II) dicarboxylates.

We have demonstrated the paramagnetic properties of **1a**, **1b**, **3a**, and **3b**, as elucidated by magnetic measurements

(SQUID), whereas **2a** and **2b** were found to be diamagnetic.

It is expected that isomorphous complexes will be synthesized using chromium, tungsten, ruthenium, rhenium, rhodium, etc. instead of copper, zinc, and nickel. Similar systems may also be designed and constructed using other sets of ligands and transition metals. Furthermore, from the perspective of molecular architecture, this strategy advances functional material science based upon complex chemistry and the nature of transition metals.

We thank Nihon Bruker AXS K.K. for its support. We also acknowledge Dr. Kenji Yoza for his assistance in the X-ray crystal examination of **3a** and **3b**.

This work was supported by a grant-in-aid from the New Energy and Industrial Technology Development Organization (NEDO).

### References

- 1 a) A. F. Constedt, *Akad. Hantl. Stockholm*, **18**, 120 (1756). b) A. Damour, *Ann. Mines*, **17**, 191 (1840).
- 2 a) R. K. Iler, "The Chemistry of Silica," Wiley, New York (1979); R. Szostack, "Molecular Sieves," 2nd ed., Blackie Academic and Professional, London (1998). b) L. L. Henchi and D. R. Ulrich, "Ultrastructure Processing of Ceramics, Glasses, and Composites," Wiley, New York (1984). c) R. E. Grim, "Applied Clay Mineralogy," McGraw-Hill, New York (1962). d) R. F. Lobo et al. (Eds.), "Microporous and Macroporous Materials," Materials Research Society, Pittsburgh (1996).
- 3 W. Mori, F. Inoue, K. Yoshida, H. Nakayama, S. Takamizawa, and M. Kishita, *Chem. Lett.*, **1997**, 1219.
- 4 S. Takamizawa, W. Mori, M. Furihata, S. Takeda, and K. Yamaguchi, *Inorg. Chem. Acta*, **283**, 268 (1998).
- 5 a) S. Takamizawa, K. Yamaguchi, and W. Mori, *Inorg. Chem. Commun.*, **1**, 177 (1998). b) S. Takamizawa, T. Ohmura, K. Yamaguchi, and W. Mori, *Mol. Cryst. Liq. Cryst.*, **342**, 199 (2000).
- 6 M. Eddaoudi, J. Kim, N. Rosi, D. Vodak, J. Wachter, M. O'Keeffe, and O. M. Yaghi, *Science*, **295**, 18 (2002).
- 7 a) S. Noro, R. Kitaura, M. Kondo, S. Kitagawa, T. Ishii, H. Matsuzaka, and M. Yamashita, *J. Am. Chem. Soc.*, **124**, 2568 (2002). b) R. Kitaura, S. Kitagawa, Y. Kubota, T. C. Kobayashi, K. Kindo, Y. Mita, A. Matsuo, M. Kobayashi, H.-C. Chang, T. C. Ozawa, M. Suzuki, M. Sakata, and M. Takata, *Science*, **298**, 2358 (2002).
- 8 S.-Y. Chui, S. M.-F. Lo, S. S.-Y. Chui, L.-Y. Shek, Z. Lin, X. X. Zhang, G.-H. Wen, and I. D. Williams, *J. Am. Chem. Soc.*, **122**, 6293 (2000).
- 9 K. Biradha and M. Fujita, *Chem. Commun.*, **2002**, 1866.
- 10 T. Ohmura, W. Mori, M. Hasegawa, T. Takei, and A. Yoshizawa, *Chem. Lett.*, **32**, 34 (2003).
- 11 W. R. Angus, J. Favède, J. Hoarau, and A. Pacault, "LANDOLT-BÖRNSTEIN," Eigenschaften Der Materie in Ihren Aggregatzuständen, 10. Teil, Magnetische Eigenschaften II, Berlin, Heidelberg, New York, Springer-Verlag (1967).
- 12 S. Noro, R. Kitaura, M. Kondo, S. Kitagawa, T. Ishii, H. Matsuzaka, and M. Yamashita, *J. Am. Chem. Soc.*, **124**, 2568 (2002).
- 13 G. B. Deacon and R. J. Phillips, *Coord. Chem. Rev.*, **33**, 227 (1980).
- 14 S. Brunauer, L. S. Deming, W. E. Deming, and E. Teller, *J.*

*Am. Chem. Soc.*, **62**, 1723 (1940).

15 R. E. Del Sesto, A. M. Arif, and J. S. Miller, *Inorg. Chem.*, **39**, 4894 (2000).

16 R. E. Lobo, J. S. Beck, S. L. Snib, D. R. Corbin, M. E. Davis, L. E. Iton, and S. I. Zones (eds.), "Microporous and Macroporous Materials," Materials Research Society Symp. Proc.,

Vol. 431, Materials Research Society, Pittsburgh, PA (1996), and refs. therein; F. Rodriguez-Reinoso, J. Rouquerol, K. S. W. Sing, and K. K. Unger (eds.), "Characterization of Porous Solids II," Studies in Surface Science and Catalysis, Vol. 62, Elsevier, Amsterdam (1991), and refs. therein.